Nanoformulation of Pheophorbide-a for Photodynamic Therapy in a Human Lung Cancer Spheroid Model

K Moloudi[1], H Abrahamse[1], B P George[1*]

[1]Laser Research Centre (LRC) Department of Health Science, Doornfontein Campus, 2028, University of Johannesburg, Johannesburg, South Africa

*Correspondence: blassang@uj.ac.za; Tel.: +27-11-599-6926

Abstract. Pheophorbide a (PPBa) is a natural compound derived from chlorophyll, and its photophysical and photochemical properties make it useful as a photosensitizer for photodynamic therapy (PDT). However, stability of PPBa in biological environments and its bioavailability are crucial for effective therapy. Nanoparticle (NP) formulation of PPBa can improve its solubility and stability. The aim of this study is to make use of liposomal nanocomplex of PPBa as photosensitizer in PDT (660 nm at 15 J/cm^2 fluency) on A549 spheroid cells. Thin-film hydration method was used for synthesis of NPs. Characterization of Lipo@PPBa were carried out using UV-Vis spectroscopy, TEM, SEM, FTIR and DLS. Moreover, cytotoxicity of NPs was evaluated at various concentrations via MTT assay. The IC50 dose was determined to assess the phototoxic effects induced by 660 nm laser irradiation at an energy density of 15 J/cm². UV-Vis spectroscopy showed a specific peak at 220 nm for lipids and two peaks for PPBa at 400 nm and 670 nm, respectively. TEM and SEM images illustrated the 45 nm size and wavy crest shape of NPs respectively. DLS data showed that the NPs have positive surface charge with zeta potential of $+6.13 \pm 4.7$ mV. MTT assay indicated that IC_{50} of Lipo@PPBa nanocomplex in dark and PDT and dark was 10 µg/mL and 7.5 µg/mL, respectively. In conclusion, Lipo@PPBa showed significant phototoxic effects on A549 spheroid cells. However, more investigations on targeted therapy using Lipo@PPBa is recommended.

1. Introduction

Lung cancer remains a significant global health challenge, with projections indicating a substantial increase in cases and deaths by 2050. Sharma et al estimate 3.8 million new cases and 3.2 million deaths globally by 2050 [1], while Guo et al. (2024) predict approximately 2.13 million cases and 1.61 million deaths in China and the United States [2]. Lung cancer cases in South Africa were approximately 6,877 in 2022 and are projected to rise to 7,924 by 2025 and 10,120 by 2030 [3]. Common treatment modalities include surgery, chemotherapy, radiotherapy, targeted therapy, and immunotherapy [4]. However, lung cancer is still a significant public health issue despite significant advancements in clinical diagnosis and treatment in recent decades.

Photodynamic therapy (PDT) is a promising treatment for lung cancer, involving photosensitizing agents activated by light to generate toxic oxygen radicals [5]. It has shown efficacy in treating early-stage non-small cell lung cancer (NSCLC), particularly for endobronchial tumors [6]. PDT for lung cancer faces several challenges despite its potential as a targeted treatment. These include limited light penetration in deep tissues, reliance on oxygen in hypoxic tumors, and the need for precise treatment planning [7]. Clinical studies have shown that PDT can prolong survival in inoperable lung cancer patients and improve quality of life. However, PDT remains underutilized in lung cancer treatment due to insufficient clinical research evaluating its effectiveness and side effects [8]. Future developments in photosensitizer (PS) design potentially aided by nanotechnology, may help address these challenges and expand PDT's clinical application in lung cancer therapy [9, 10].

Liposomal formulations of PSs such as pyropheophorbide-a and its derivatives have shown promise for enhancing PDT in cancer treatment. These formulations improve drug delivery, by increasing intracellular uptake up to 5-fold compared to free PSs [11]. Liposomal encapsulation also addresses the poor water solubility of porphyrins, enhancing their bioavailability and prolonging blood circulation [12]. Studies have demonstrated that liposomal porphyrins are more effective than free forms in inducing apoptosis in cancer cell lines [13].

In this study, a liposomal nanoformulation of pheophorbide-a (Lipo@PPBa) was employed in PDT using a 660 nm laser to treat A549 spheroid cells *in vitro*, Figure 1. The hypothesis of this study is that Lipo@PPBa can enhance the PDT efficacy by improving PPBa delivery and cellular uptake and promoting cell death in A549 spheroid cells.

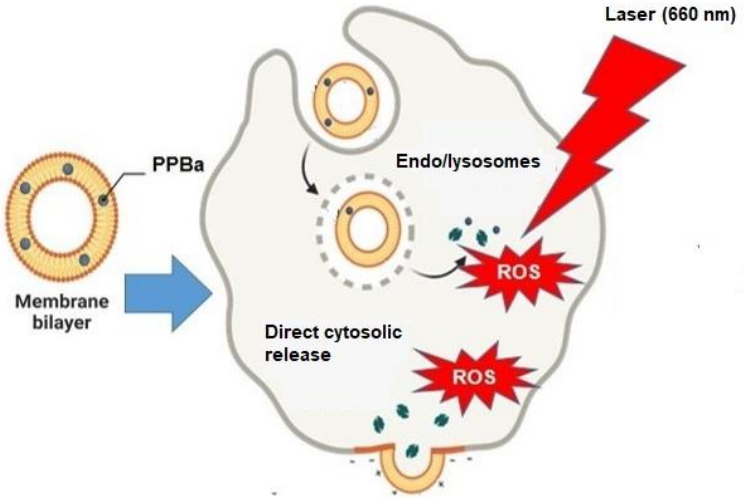

Figure .1. The liposome-based Lipo@PPBa nanocomplex, following cellular internalization and exposure to 660 nm laser irradiation, facilitates endo/lysosomal escape or direct cytosolic release in A549 cells for effective PDT.

2. Materials and methods

2.1. Materials

The following reagents and materials were procured in South Africa: pheophorbide-a (16072, powder, >95% purity, Biocom Africa), MTT (11465007001, Sigma), cholesterol (C8667, Sigma), DSPC (P1138-1G, Sigma), Dulbecco's Modified Eagle Medium (DMEM, D5796, Thermo Fisher), chloroform (C2432, Sigma), Fetal Bovine Serum (FBS, Thermo Fisher), TrypLE (12604013, Thermo Fisher), dimethyl sulfoxide (DMSO, Thermo Fisher), phosphate-buffered saline (PBS, Thermo Fisher), 96-well ultra-low attachment plates (174929, Thermo Fisher), crystal violet (C0775, powder, >90% purity, Thermo Fisher), and DAPI (D3571, Thermo Fisher).

2.2. Synthesis and characterization of Lipo@PPBa complex

Lipo@PPBa were synthesized by the thin-film hydration method [14, 15]. Briefly, DSPC (80 mg) and cholesterol (30 mg) were dissolved in chloroform, followed by solvent evaporation using a rotary evaporator for 70 min (at 75 °C and 65 rpm). The resulting samples of NPs were then stored at 8 °C for further characterization. To analyze

and characterization of the Lipo@PPBa complex, various techniques were employed, including UV-Vis spectrophotometry, FTIR, dynamic light scattering (DLS), Transmission Electron Microscopy (TEM) and Scanning Electron Microscopy (SEM).

2.3. Spheroid cell culture and treatment

A549 lung cancer cell line (ATCC CCL-185), after the third passage, was harvested and counted using an automated cell counter. A total of 1,000 cells per well were then seeded into ultra-low attachment 96-well plates using DMEM) supplemented with 10% FBS and 1% penicillin-streptomycin (Sigma, USA). Plates were centrifuged at 1,000 rpm for 5 min to facilitate cell aggregation at the bottom. The cells were incubated at 37 °C in a humidified incubator with 5% CO_2 and 95% of O_2, and medium refreshed every other day. Once the spheroids reached an average diameter of approximately 400 µm after 3 days, they were exposed to varying concentrations (0–12 µg/mL) of Lipo@PPBa, with or without PDT (660 nm laser, 15 J/cm²). After 24 h, the spheroids were washed three times with PBS (1X), dissociated, and subjected to cytotoxicity, colony formation, and nuclear fragmentation assays.

2.3.1. Photodynamic therapy (PDT)

To assess the PDT potential of Lipo@PPBa, its IC_{50} dose (10 µg/mL) was applied in combination with 660 nm laser at a total fluence of 15 J/cm².The light source used was a high-power diode laser (300 mA, RGBLase LLC, 101090908), provided by the National Laser Centre. Laser output in milliwatts was determined using a Coherent® FieldMate Power Meter (1098297) coupled with a PM3 thermopile sensor (1098336, ALP – Applied Laser Power, South Africa). These values were used in equations (1), (2), and (3) to determine the appropriate irradiation time. A549 spheroids were prepared by seeding 1×10^3 cells per well in a 96-well ultra-low attachment plate and incubated for three days prior to treatment. Following this, spheroids were treated with Lipo@PPBa under PDT conditions. The laser beam, with a spot diameter of 3.4 cm (1.7 cm radius), was sufficient to cover four wells at once. The exposure time (in min) was determined using the specified equations:

$$\text{Intensity (W/cm}^2\text{)} = \text{Energy/Area} = 100\ \text{mW} / 3.14\text{x}1.72\ \text{cm} = 0.011\ \text{W/cm}^2 \quad (1)$$

$$\text{Area} = \pi r^2 = 3.14\text{x}1.72 = 9.074\ \text{cm}^2 \quad (2)$$

$$\text{Exposure time (min)} = \text{Dose (J/cm}^2\text{)/Intensity (W/cm}^2\text{)} = 15/0.011 = 10.82 \simeq 22.72\ \text{min} \quad (3)$$

2.3.2. MTT assay and IC_{50} of Lipo@PPBa complex

The cytotoxic effects of Lipo@PPBa at varying concentrations (0, 2, 4, 6, 8, 10, and 12 µg/mL) on A549 spheroids, both without and with PDT (660 nm laser, 15 J/cm²), were evaluated using the MTT assay and ELISA (Perkin-Elmer, Midrand, South Africa. Briefly, the culture medium was removed, spheroids were rinsed with 1× PBS, and dissociated into single cells using 200 µL of TrypLE (1×) for 5 min. The cell suspension was washed with PBS and seeded into 96-well plates at a concentration of 2×10^4 cells/mL. Cells were incubated overnight at 37 °C in a humidified atmosphere containing 5% CO_2. After removing the medium, 20 µL of MTT solution (Sigma, USA) was added to each well and the plate was incubated for an additional 4 h. Cell viability was then quantified based on absorbance using equation (4):

$$\%\ \text{survival} = (\text{OD of experimental sample}) / (\text{OD of control sample}) \times 100. \quad (4)$$

2.3.3. Colony formation assay

The colony formation assay was employed to evaluate the clonogenic potential of individual A549 cells following treatment. Spheroids were exposed to the IC_{50} concentration (10 µg/mL) of Lipo@PPBa followed by irradiation (660 nm laser, 15 J/cm²), then dissociated using 200 µL of TrypLE to obtain single cells. A total of 1,000 cells were seeded into each well of a 6-well plate (M8562) containing DMEM and incubated for 14 days to allow colony formation. After the incubation, colonies were fixed using 5% formaldehyde and stained with 0.5% crystal violet for visualization. Colonies were imaged and quantified using an Inverted microscope and ImageJ software (version 1.48v). A colony was defined as a cluster containing at least 50 cells.

2.3.4. Nuclear fragmentation assay

The nuclear fragmentation assay, a method used to identify apoptotic features such as chromatin condensation and nuclear breakage, [16] was conducted on A549 spheroids treated with the IC_{50} dose (10 µg/mL) of Lipo@PPBa alone and following PDT. After treatment, the spheroids were washed three times with 1× PBS and dissociated using 200 µL of TrypLE. Approximately 1×10^5 cells were then seeded onto glass coverslips and fixed using 5% formaldehyde. The fixed cells were washed three times with PBS and permeabilized with 100 µL of 0.5% Triton

X-100 in PBS for 15 min at room temperature. Subsequently, after additional PBS washes, cells were stained with 100 µL of DAPI solution (1 µg/mL in PBS) and incubated for 15 min in the dark at room temperature. Excess dye was removed with three PBS washes, and nuclear morphology was visualized using a fluorescence microscope (Wirsam Olympus CKX41) equipped with a DAPI filter (excitation ~358 nm, emission ~461 nm).

3. Statistical Analysis

Statistical analysis was conducted using one-way ANOVA followed by Tukey's post-hoc test in SPSS software (version 22). All experiments were performed in triplicate (n=3) and data are expressed as mean values ± SD (standard deviation). The value of $p^{*} < 0.05$, $p^{**} < 0.01$ was considered to be statistically significant.

4. Results and Discussion

4.1. Characterization of Lipo@PPBa

UV-vis spectroscopy revealed that the Lipo@PPBa complex exhibited an absorption peak ~220 nm, along with two distinct peaks corresponding to PPBa at approximately 400 nm and 670 nm (Figure 2A), as previously reported [17, 18]. FTIR analysis further supported the successful encapsulation of PPBa. showing four notable peaks at 1351, 1600, 2736, and 2907 cm^{-1} for the liposomes, while free PPBa displayed five absorption bands at 670, 900, 1395, 1680, and 2922 cm^{-1}. Moreover, the Lipo@PPBa complex exhibited similar FTIR peaks at 1351, 1600, 2736, and 2907 cm^{-1} (Figure 2B). Similar spectral behavior was reported by Rani et al., where overlapping FTIR peaks confirmed the integration of therapeutic agents into lipid-based nanocarriers without significant chemical modification [19].

TEM analysis showed that the Lipo@PPBa complex had an average size of approximately 45.7 nm (Figure 2C). The SEM image and backscattered electron (BSE) image also illustrated a wavy morphology of the Lipo@PPBa complex (Figure 2D and E) and confirmed its successful loading onto the liposomes. Moreover, DLS analysis revealed that incorporating PPBa into liposomes led to an increase in particle size from 100.5 ± 3 nm to 251.8 ± 12 nm and a reduction in zeta potential from $+17.01 \pm 7$ mV to $+6.13 \pm 4.7$ mV (Table 1). However, morphological analysis using TEM revealed an average particle size of ~45.7 nm, which is smaller than the hydrodynamic diameter measured by DLS (251.8 ± 12 nm). This discrepancy is commonly observed and attributed to the hydration shell measured by DLS, as also reported previously [20, 21]. TEM-based sizes typically reflect the dry-state diameter, while DLS accounts for solvation and potential particle aggregation in solution.

Finally, DLS analysis showed an increase in particle size and a notable decrease in zeta potential after PPBa encapsulation, indicating changes in surface charge and colloidal stability. This trend aligns with findings by Cheng et al [22], who observed reduced zeta potential upon drug loading due to shielding of surface charges and increased particle aggregation potential. The observed zeta potential of $+6.13 \pm 4.7$ mV in Lipo@PPBa suggests moderate stability, suitable for short-term systemic delivery.

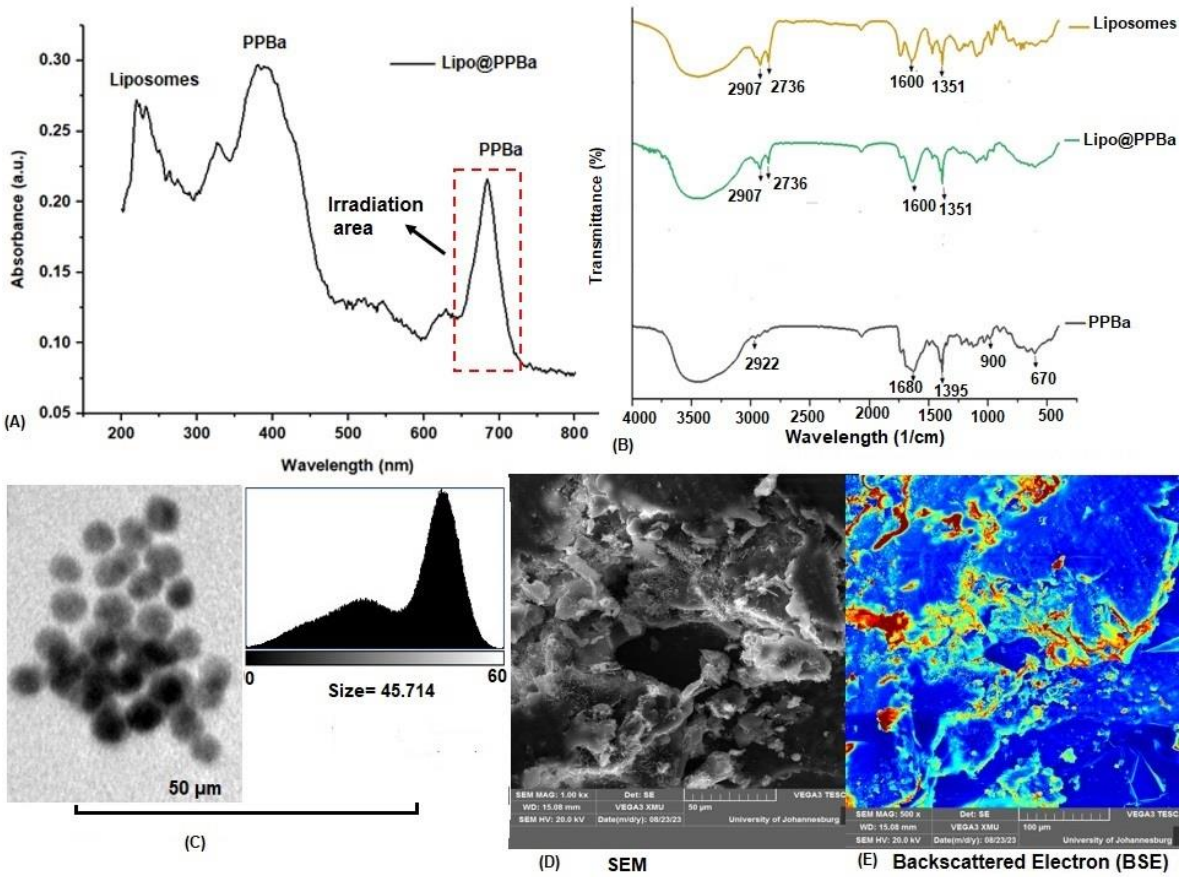

Figure .2. Various characterization tests for Lipo@PPBa nanocomplex: (A) UV-spectroscopy, (B) FTIR, (C) TEM (C), (D) SEM image and (E) backscattered electron (BSE)

Table 1. DLS data has been summarized.

Nanostructures	Size (nm)	Zeta potential (mV)	PDI
Liposomes	100.5±3	+17.01±7	0.238
Lipo@PPBa	251.8±12	+6.13±4.7	0.410

4.2. Cyto and phototoxicity of Lipo@PPBa

The cytotoxic effects of Lipo@PPBa at different concentrations (0–14 µg/mL) were evaluated in A549 spheroid cells using the MTT assay after 24 h post treatment (Figure 3). As can be seen, cell viability for control, 2, 4, 6, 8, 10, 12 and 14 µg/mL concentration of Lipo@PPBa alone (without PDT) was 100%, 91.7%, 80.5%, 72.1%, 61.3%, 51.6%, 43.4 and 34%, receptively (Figure 3A and B). Lipo@PPBa at the concentrations more than 4 µg/mL had significant toxicity compared with control group ($p<0.05$). These findings suggest that Lipo@PPBa possesses inherent cytotoxicity at elevated doses, even in the absence of light activation. Additionally, viability percentage for laser alone and Lipo@PPBa at various concentrations of 2, 4, 6, 8, 10, 12, 14 µg/mL post-PDT (15 J/cm^2) was 91%, 84%, 71%, 56%, 45%, 35%, 28% and 19%, respectively, (Figure 3C). The calculated IC_{50} of Lipo@PPBa post-PDT was 7.5 µg/mL compared to 10 µg/mL in dark. Notably, the data showed that the IC_{50} value post-PDT was 7.5 µg/mL, which is significantly lower than the IC_{50} under dark conditions (10 µg/mL), confirming that photodynamic activation enhances therapeutic efficacy. Additionally, the threshold dose (Td) of Lipo@PPBa, defined as the minimum concentration required to produce significant cytotoxicity [23], was identified as 4 µg/mL (Figure 3D). These results collectively highlight that Lipo@PPBa exerts greater cytotoxic effects when activated by light and suggest its potential as an effective agent for PDT-based cancer therapy. The dose-dependent reduction in viability also supports further optimization of treatment concentrations to maximize efficacy while minimizing off-target effects.

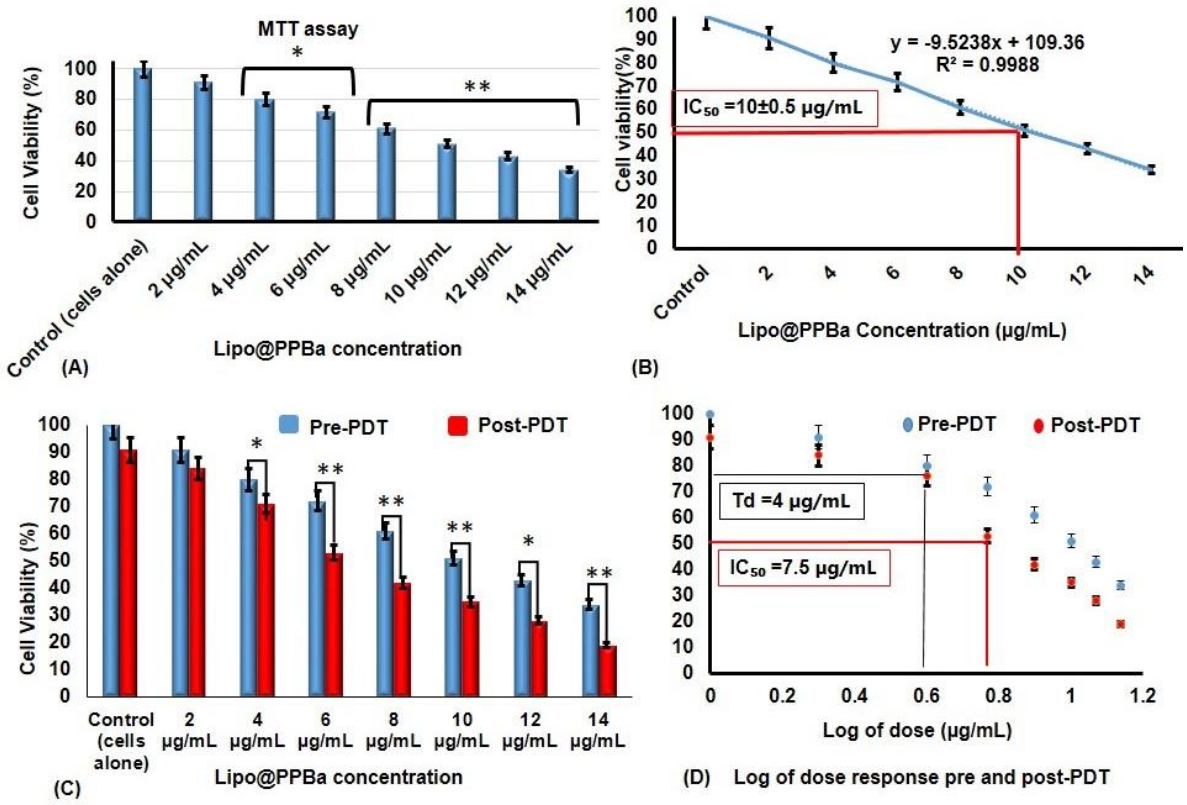

Figure .3. (A, B), MTT assay (cytotoxicity) and regression model of Lipo@PPBa, after 24 h. (C), cytotoxicity of Lipo@PPBa post-PDT, (D), Sigmoid model for Lipo@PPBa with and without PDT on A549 cancer cells. Data represents as mean ± SD of three independent experiments, ($p^{*} < 0.05$, $p^{**} < 0.01$).

4.3. Morphology, colony formation assay and nuclear fragmentations

Morphology (Figure 4A) and live/dead assay (Figure 4A) of spheroids illustrated that IC_{50} of Lipo@PPBa nanocomplex post-PDT caused shrinkage, dissociation and suppression of spheroids in comparison to other groups such as control, laser (alone) and IC_{50} of Lipo@PPBa nanocomplex in dark. Furthermore, cells treated with the IC_{50} concentration of Lipo@PPBa under PDT exhibited prominent nuclear fragmentation (Figure 4C). This effect was clearly visible under microscopic observation and indicated advanced stages of cell death. The extent of nuclear fragmentation in this group was significantly higher compared to the other groups. Finally, colony formation results demonstrated that the IC_{50} concentration of Lipo@PPBa reduced cell survival to 38±4 %, while for other groups such as control, laser and Lipo@PPBa was 100%, 88% and 51%, respectively, (Figure 4D and E). These findings highlight the enhanced cytotoxic effect of photoactivated Lipo@PPBa compared to non-irradiated and untreated conditions.

This outcome aligns with previous studies highlighting the effectiveness of PS-loaded nanocarriers in enhancing PDT outcomes. For instance, Zhang et al. (2022) reported that a curcumin-loaded nanoparticle system under PDT reduced the clonogenic survival of MCF-7 breast cancer cells to below 40%, consistent with the results obtained here using Lipo@PPBa [24]. Similarly, Zeng et al. (2021) demonstrated that Ce6-loaded lipid nanoparticles achieved about 35% survival in A549 cells under similar laser exposure conditions, indicating comparable efficacy in terms of colony inhibition [25].

However, the results validate the effectiveness of Lipo@PPBa as a promising nanocarrier capable of significantly impairing cancer cell proliferation when appropriately activated.

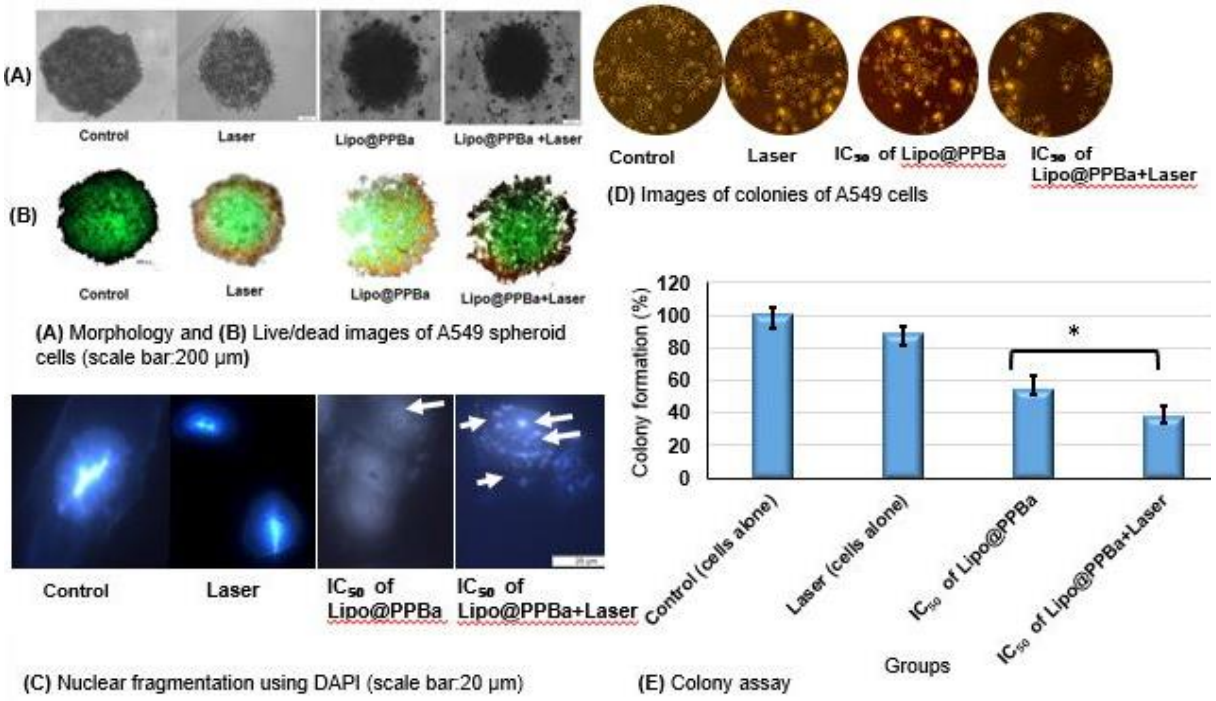

Figure 3. Various assessments of spheroid response to treatment: (A) shows the morphology of spheroids under a light microscope, (B) presents live/dead fluorescence images where green indicates live cells and red indicates dead cells, (C) displays nuclear fragmentation visualized using DAPI staining, (D) shows representative images of colony formation, and (E) quantifies the percentage of colony formation, ($p^* < 0.05$).

5. Conclusion

The nanoformulation of PPBa into liposomal carriers (Lipo@PPBa) demonstrates significant potential as a targeted and effective PS for PDT in a 3D human lung cancer spheroid model. Physicochemical characterization confirmed successful encapsulation of PPBa, favorable particle size, and stability, while optical analyses verified the retention of Lipo@PPBa's photodynamic properties. Compared to the non-irradiated formulations, light-activated Lipo@PPBa exhibited markedly enhanced cytotoxic effects, and a more pronounced inhibition of colony formation *via* nuclear fragmentation. These findings illustarte the importance of nanoparticle-based delivery systems in overcoming the limitations of conventional PDT and highlight Lipo@PPBa as a promising candidate for further preclinical development in lung cancer therapy.

6. Acknowledgements

This work is based on the research funded by the South African Research Chairs initiative of the Department of science and technology and National Research Foundation (NRF) of South Africa (Grant No. 98337), South African Medical Research Council (Grant No. SAMRC EIP007/2021), as well as grants received from the NRF Research Development Grants for Y-Rated Researchers (Grant No: 137788), University Research Committee (URC), African Laser Centre (ALC), CSIR African Laser Centre research grant (HLHA26X Task ALC-R001), University of Johannesburg, and the Council for Scientific Industrial Research (CSIR)-National Laser Centre (NLC).

References:

[1] Sharma R. 2022 Mapping of global, regional and national incidence, mortality and mortality-to-incidence ratio of lung cancer in 2020 and 2050.Available from International Journal of Clinical Oncology.**27**:665-75.

[2] Guo L, Zhu C, Cai L, Zhang X, Fang Y, Chen H, et al. 2024 Global burden of lung cancer in 2022 and projected burden in 2050.Available from Chinese Medical Journal.**137**:2577-82.

[3] Finestone E, Wishnia J. 2022 Estimating the burden of cancer in South Africa.Available from SA Journal of Oncology.**6**:220.

[4] Salmani-Javan E, Jadid MFS, Zarghami N. 2024 Recent advances in molecular targeted therapy of lung cancer: Possible application in translation medicine.Available from Iranian Journal of Basic Medical Sciences.**27**:122.
[5] Moloudi K, Abrahamse H, George BP. 2024 Co-delivery of berberine and gold nanoparticles on liposomes for photodynamic therapy against 3D lung cancer cells.Available from Materials Advances.**5**:6185-95.
[6] Simone CB, Friedberg JS, Glatstein E, Stevenson JP, Sterman DH, Hahn SM, et al. 2012 Photodynamic therapy for the treatment of non-small cell lung cancer.Available from Journal of thoracic disease.**4**:63.
[7] Jankun J. 2019 A thousand words about the challenges of photodynamic therapy: Challenges of photodynamic therapy.Available from Journal of Medical Science.**88**:195-9.
[8] Wang K, Yu B, Pathak JL. 2021 An update in clinical utilization of photodynamic therapy for lung cancer.Available from Journal of Cancer.**12**:1154.
[9] Zhao X, Liu J, Fan J, Chao H, Peng X. 2021 Recent progress in photosensitizers for overcoming the challenges of photodynamic therapy: from molecular design to application.Available from Chemical Society Reviews.**50**:4185-219.
[10] Moloudi K, Abrahamse H, George BP. 2024 Application of liposomal nanoparticles of berberine in photodynamic therapy of A549 lung cancer spheroids.Available from Biochemistry and biophysics reports.**40**:101877.
[11] Guelluy P-H, Fontaine-Aupart M-P, Grammenos A, Lécart S, Piette J, Hoebeke M. 2010 Optimizing photodynamic therapy by liposomal formulation of the photosensitizer pyropheophorbide-a methyl ester: in vitro and ex vivo comparative biophysical investigations in a colon carcinoma cell line.Available from Photochemical & Photobiological Sciences.**9**:1252-60.
[12] Zhou H, Xia L, Zhong J, Xiong S, Yi X, Chen L, et al. 2019 Plant-derived chlorophyll derivative loaded liposomes for tri-model imaging guided photodynamic therapy.Available from Nanoscale.**11**:19823-31.
[13] Temizel E, Sagir T, Ayan E, Isik S, Ozturk R. 2014 Delivery of lipophilic porphyrin by liposome vehicles: Preparation and photodynamic therapy activity against cancer cell lines.Available from Photodiagnosis and photodynamic therapy.**11**:537-45.
[14] Ai X, Zhong L, Niu H, He Z. 2014 Thin-film hydration preparation method and stability test of DOX-loaded disulfide-linked polyethylene glycol 5000-lysine-di-tocopherol succinate nanomicelles.Available from asian journal of pharmaceutical sciences.**9**:244-50.
[15] Xiang B, Cao D-Y. 2021 Preparation of drug liposomes by thin-film hydration and homogenization.Available from Liposome-based drug delivery systems:25-35.
[16] Alshiraihi I, Kato TA.2022 Apoptosis detection assays. Chromosome Analysis: Methods and Protocols: Springer. p. 53-63.
[17] Kim M-J, Jang D-H, Lee Y-I, Jung HS, Lee H-J, Choa Y-H. 2011 Preparation, characterization, cytotoxicity and drug release behavior of liposome-enveloped paclitaxel/Fe3O4 nanoparticles.Available from Journal of nanoscience and nanotechnology.**11**:889-93.
[18] Moloudi K, Abrahamse H, George BP. 2025 Liposomes-based co-delivery of pheophorbide a and gold nanoparticles for thermo-photodynamic therapy purpose on lung cancer spheroids.Available from Results in Chemistry.**15**:102234.
[19] Rani A, Kaur R, Aldahish A, Vasudevan R, Balaji P, Dora CP, et al. 2025 Nanostructured Lipid Carriers (NLC)-Based Topical Formulation of Hesperidin for Effective Treatment of Psoriasis.Available from Pharmaceutics.**17**:478.
[20] Li R-T, Chen M, Yang Z-C, Chen Y-J, Huang N-H, Chen W-H, et al. 2022 AIE-based gold nanostar-berberine dimer nanocomposites for PDT and PTT combination therapy toward breast cancer.Available from Nanoscale.**14**:9818-31.
[21] Li L, Nurunnabi M, Nafiujjaman M, Lee Y-k, Huh KM. 2013 GSH-mediated photoactivity of pheophorbide a-conjugated heparin/gold nanoparticle for photodynamic therapy.Available from Journal of Controlled Release.**171**:241-50.
[22] Cheng C, Wu Z, McClements DJ, Zou L, Peng S, Zhou W, et al. 2019 Improvement on stability, loading capacity and sustained release of rhamnolipids modified curcumin liposomes.Available from Colloids and surfaces B: biointerfaces.**183**:110460.
[23] Nascarella MA, Calabrese EJ. 2009 The relationship between the IC50, toxic threshold, and the magnitude of stimulatory response in biphasic (hormetic) dose–responses.Available from Regulatory Toxicology and Pharmacology.**54**:229-33.
[24] Zhang L, Chen D, Yu D, Regenstein JM, Jiang Q, Dong J, et al. 2022 Modulating physicochemical, antimicrobial and release properties of chitosan/zein bilayer films with curcumin/nisin-loaded pectin nanoparticles.Available from Food Hydrocolloids.**133**:107955.

[25] Zeng Q, Ma X, Song Y, Chen Q, Jiao Q, Zhou L. 2022 Targeting regulated cell death in tumor nanomedicines.Available from Theranostics.**12**:817.